Annals of Glaciology

Article

Cite this article: Perovich D, Light B, Dickinson S (2020). Changing ice and changing light: trends in solar heat input to the upper Arctic ocean from 1988 to 2014. *Annals of Glaciology* **61**(83), 401–407. https://doi.org/10.1017/aog.2020.62

Received: 30 November 2019
Revised: 27 July 2020
Accepted: 31 July 2020
First published online: 19 October 2020

Keywords:
Sea ice; sea-ice growth and decay; surface mass budget

Author for correspondence:
Don Perovich,
E-mail: donperovich@gmail.com

cambridge.org/aog

Changing ice and changing light: trends in solar heat input to the upper Arctic ocean from 1988 to 2014

Donald Perovich[1], Bonnie Light[2] and Suzanne Dickinson[2]

[1]Thayer School of Engineering, Dartmouth College, Hanover, NH 03755, USA and [2]Polar Science Center, University of Washington, Seattle, WA 98105, USA

Abstract

The Arctic sea-ice cover has undergone a significant decline in recent decades. The melt season is starting earlier, ice is thinner and seasonal ice dominates. Here we examine the effects of these changes on the solar heat input to the upper ocean in ice-covered Arctic waters from 1985 to 2014. Satellite observations of ice concentration, onset dates of melt and freeze-up and ice age, are combined with ice thicknesses from the PIOMAS model and incident solar irradiance from reanalysis products to calculate the contributions of open ocean and ice to the solar heat input in the upper ocean. Of the total, 86% of the area has positive trends for solar heat input to the ocean through leads due to decreases in ice concentration. Only 62% of the area shows positive trends of solar heat input to the ocean explicitly through the ice. Positive trends are due to thinning ice, while negative trends occur in regions where the ice-free season has lengthened. The annual total solar heat input to the ocean exhibits positive trends in 82% of the area. The spatial pattern of the cumulative annual total solar heat input is similar to the pattern of solar heat input directly to leads.

Introduction

The decline of the Arctic sea-ice cover over the past few decades is well established (Richter-Menge and others, 2018). There has been a decrease in ice extent in all months, most prominently in September (Stroeve and others, 2012; Meier and others, 2014). There has also been a general shift from older, thicker ice to younger, thinner ice (Maslanik and others, 2011; Comiso, 2012; Tschudi and others, 2016; King and others, 2017; Kwok, 2018; Kwok and others, 2019). Several mechanisms have been proposed and evaluated for this decline including general surface warming (Serreze and others, 2009), changes in cloud conditions (Kay and Gettelman, 2009), atmospheric pressure patterns (Overland and Wang, 2005), ice dynamics (Hutchings and Rigor, 2012) and solar radiation (Perovich and others, 2008).

Assessing the role of solar radiation in the surface heat budget, Perovich (2005) determined the annual partitioning of solar radiation between reflection to the atmosphere (68%), absorption in the ice (24%) and transmission to the ocean (8%) using data from the SHEBA field campaign (Uttal and others, 2002). Mass-balance measurements were used with solar partitioning calculations to establish a relationship between bottom melt and solar heat input to open ocean (Perovich and others, 2008, 2011). Arndt and Nicolaus (2014) examined the spatial and temporal distribution and variability of light transmission through the sea ice to the ocean, finding an increase of 1.5% a^{-1}. They also found that 96% of the light transmission through the ice occurs from May through August. Nicolaus and others (2012) showed that transmittance through a first-year ice cover was three times greater than through a multiyear ice cover, due in large part to the larger pond fraction on seasonal ice.

Here we examine the solar heat input to the upper ocean, including heat directly deposited into the open ocean as well as sunlight transmitted through the ice. Daily solar heat input into the open ocean and through the ice is computed every day from 1985 to 2014 on a 25 km × 25 km Equal-Area Scalable Earth grid. Annual cumulative values are computed, the relative contributions from open ocean and ice are calculated, temporal trends are derived, and the drivers of these trends are assessed.

Approach

At any site, the total solar heat input to the upper ocean (Q_{tot}) consists of contributions from sunlight deposited in the open ocean (Q_{ocn}) and sunlight transmitted through the ice (Q_{ice}). This can be expressed as

$$Q_{tot} = Q_{ocn} + Q_{ice}$$

$$Q_{tot} = (Q_r)(1 - C)(1 - \alpha_{ocn}) + (Q_r)(C)(1 - \alpha_{ice})\exp(-KH_i), \quad (1)$$

where *tot* represents total, *ocn* is ocean and *r* is radiation. The first term describes the solar heat deposited in the open ocean and the second term is the solar heat transmitted through the ice

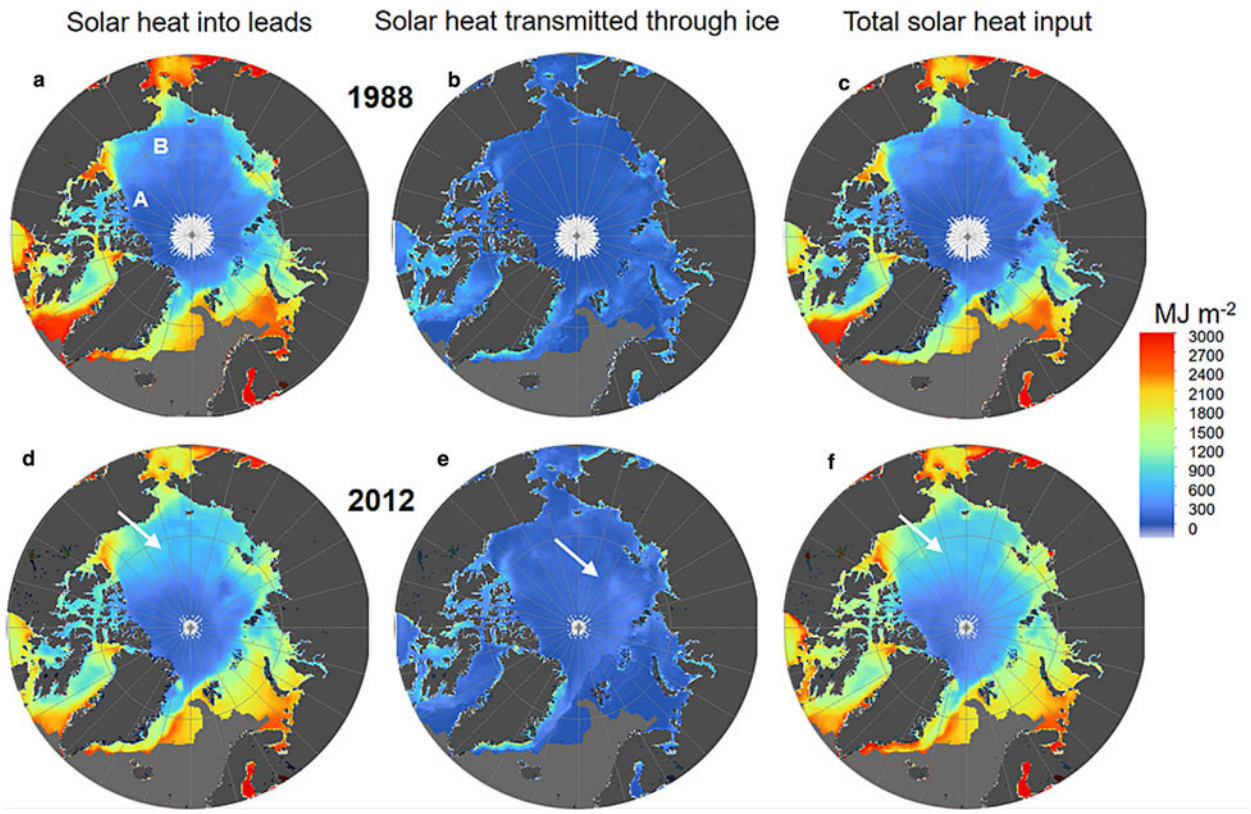

Fig. 1. Maps of cumulative annual (a, d) solar heat input to open ocean, (b, e) transmitted through the ice into the ocean, and (c, f) the total solar heat input to the ocean for 1988 (a, b, c) and 2012 (d, e, f). B denotes the Beaufort region and A the Archipelago. Arrows denote regions of interest referred to in the text.

into the ocean. Six parameters determine the solar heat input. Q_r is the daily solar energy input at the surface (MJ m^{-2}), C is the ice concentration, α_{ocn} is the albedo of open ocean, α_{ice} is the albedo of the ice cover, and H_i is the ice thickness (m). We use an exponential decay law for light loss in the ice, with an extinction coefficient K (m^{-1}).

The domain of interest includes places where there was sea ice during the period from 1985 through 2014. This region is illustrated in Figure 1. We evaluate Eqn (1) at 20 878 grid cells on the Equal Area Scalable Earth 2.0 (EASE2) grid every day from 1985 through 2014. This requires having values for the six parameters in Eqn (1) at every gridcell for every day. The first step was to build a database with the required information. Some parameters were straightforward, while others were complex. We used the MERRA reanalysis product to get values of daily solar energy input from 175 to 3850 nm. Ice concentration came from the National Snow and Ice Data Center (NSIDC-0051, http://nsidc.org/data/nsidc-0051). The open ocean albedo is set to 0.07 based on field observations by Pegau and Paulson (2001).

The parameters for calculating transmission through the ice are more complex. The sea-ice albedo is derived using albedo evolution curves for first-year ice (Perovich and Polashenski, 2012) and multiyear ice (Perovich and others, 2002). The age of the ice was obtained using the methodology and dataset of Tschudi and others (2016, 2019). The albedo evolves through five stages for multiyear ice and seven stages for first-year ice. These phases start with: dry snow, melting snow, phases of melt pond formation and evolution, and finally fall freeze-up. The effects of melt ponds are implicitly included in this treatment. The timing of these stages depends on the onset dates of snowmelt and sea-ice freeze-up, as the albedo evolution curves are either compressed or expanded to fit within the onset dates. Results from Markus and others (2009) and Stroeve and others (2014) were used to determine the onset dates.

Ice thickness values were obtained from the output of the Pan-arctic Ice/Ocean Modeling and Assimilation System (PIOMAS; Zhang & Rothrock, 2003). In this model, 12 subgrid categories are used to describe an ice thickness distribution for each gridcell, and the average thickness is assigned to Hi. Detailed information about the sea ice and ocean model components and data assimilation can be found in Schweiger and Zhang (2015) and Zhang and others (2016) and are not repeated here. We use an exponential decay law for light attenuation in the ice, with an extinction coefficient K (m^{-1}).

The value of $K = 1.0$ m^{-1} was chosen from empirical studies on light propagation through melting summer sea ice at bare ice and ponded sites (Light and others, 2008, 2015). These studies include detailed information on ice physical properties and thickness allowing an accurate extinction coefficient to be determined. Other studies have found different values of K. For example, Katlein and others (2019) analyzed spatially distributed light measurements underneath sea ice using remotely operated vehicles covering a wide range of ice conditions over 6 years and found a modal peak extinction coefficient of ~2.0 m^{-1} for the summer months. While the use of this higher value would decrease the amount of sunlight penetrating the ice, we chose the lower values extinction coefficient values as they were directly supported by detailed physical property characterizations.

Selecting a single value for K is an approximation, as different values would be expected for snow, cold ice, melting ice and melt ponds. There is not sufficient information to include a complete treatment of a spatially and temporally variable K. This is an average value of K selected to represent conditions over the seasonal cycle, with a bias towards the May through August period since that is when most light transmission occurs (Arndt and Nicolaus, 2014). We suggest $K = 1.0$ m^{-1} provides a good compromise value for a summer ice cover that is snow-free, with a mix of bare ice and melt ponds.

https://doi.org/10.1017/aog.2020.62 Published online by Cambridge University Press

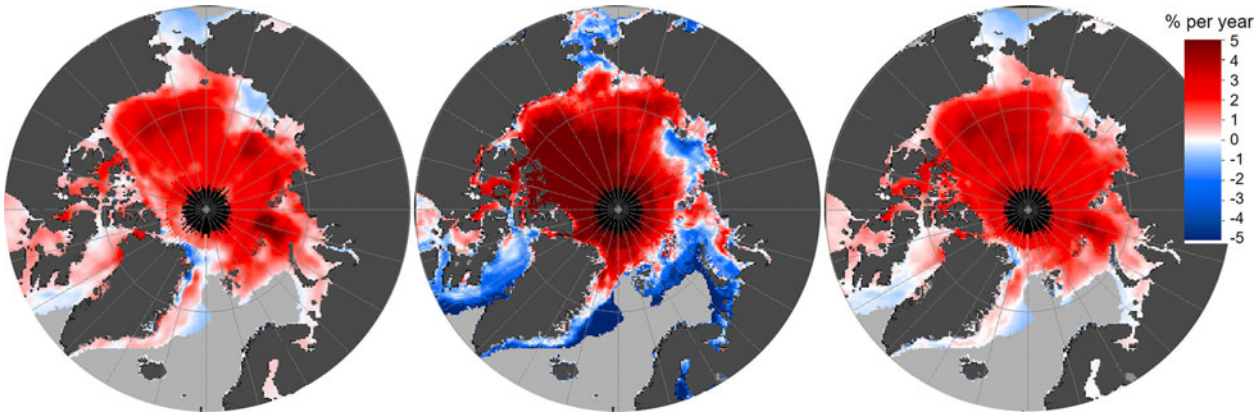

Fig. 2. Maps showing trends of (a) solar heat input to open ocean, (b) transmitted through the ice into the ocean and (c) the total solar heat input to the ocean. The units are percent per year.

We used these data to calculate the solar heat input to the ocean through the open ocean, through the ice and their sum at every gridcell for every day. Daily values were summed over the year to obtain annual totals of Q_{ocn}, Q_{ice} and Q_{tot}. There are uncertainties in the input parameters used to calculate the Q values. For example, sea-ice concentration retrievals from the passive microwave derived sea-ice concentrations are complicated by surface meltwater. These uncertainties do not have a systematic spatial or temporal bias that would significantly alter the results presented in this paper.

Results

We now examine the spatial distribution of annual cumulative values of Q_{ocn}, Q_{ice} and Q_{tot} for 2 years, 1988 and 2012. The year 1988 is representative of ice conditions early in the satellite record, while 2012 had the record minimum September ice extent. The 1988 values are plotted in Figure 1 panels a–c. In 1988 there was large spatial variability in the cumulative annual solar heat input directly to open ocean (Fig. 1a). Values around the periphery of the ice cover, where the ice is only present seasonally, were as large as 3000 MJ m^{-2}. In the Central Arctic, where ice is present year-round, values were typically less than a few hundred MJ m^{-2}. Values of the cumulative annual solar heat transmitted through the ice were relatively small and showed little spatial variability (Fig. 1b). The combined total solar heat input was dominated by the heat input through the open ocean and demonstrates the same spatial pattern, with slightly larger values due to the contribution from light transmission through the ice.

For comparison, results from 2012, the year of the smallest September ice extent of the satellite record, are plotted in Figure 1 panels d–f. The solar heat input directly into open ocean (Fig. 1d) shows a similar pattern to 1988 but with values hundreds of MJ m^{-2} larger in the Central Arctic (see arrow) and a few hundreds of MJ m^{-2} smaller in the Bering and Labrador Seas. The pattern of solar heat transmitted through the ice (Fig. 1e) is similar to 1988, but with a general increase in transmission in the Central Arctic (see arrow). In most regions, there was an increase in total solar heat in 2012 compared to 1988.

We take this analysis a step further by considering every year and examining trends. The temporal evolution of solar heat input was examined by determining the cumulative annual heat input to the ocean from the open ocean and from transmission through the ice and their sum for each year from 1985 to 2014 at each gridcell. A linear fit was applied to the time series of annual solar heat input to compute the trend at each gridcell. The results are shown in Figure 2, with red denoting positive trends (increasing heat input) and blue negative.

The trends for solar heat input to the ocean through the open ocean are strongly positive, with 86% of the area showing increasing solar heat input. The median trend was 1.3% a^{-1} and the mean was 1.2% a^{-1}. Most of the Central Arctic has positive trends of more than 1% a^{-1}, with the largest trends of up to 5% a^{-1} found north of Novaya Zemlya. Some areas, north of Greenland and around the periphery of the ice cover, show a small negative trend in solar heat through the open ocean.

The trends of solar heat input through the ice are much larger and cover a wider range of values from −10 to +10% a^{-1}. The mean trend is 1.1% a^{-1} and the median is 0.9% a^{-1}. Only 62% of the trends are positive. Trends are >5% a^{-1} in much of the western Arctic. In contrast, there are large negative trends around the periphery of the ice cover. In these areas, there is less ice present over the course of the summer. The result is an increase in heat input through the open ocean and a decrease in heat input through the ice.

The cumulative annual total solar heat input to the ocean exhibits positive trends in 82% of the area. The mean trend was an increase of 1.4% $a^{-1}$and the median was 1.1% a^{-1}. The spatial pattern is similar to the pattern of solar heat input directly to the open ocean.

We can examine which parameters are driving the trends in solar heat input to the upper ocean by narrowing our focus to results from two locations. One location is in the Beaufort Sea (76 N, 160 W), where there are large amounts of solar heat input to the ocean. This ice loss has led to several investigations exploring the thermohaline structure and heat exchange of the upper layers of the Arctic Ocean and their role in enhanced ice loss (e.g. Haynes, 2010; Toole and others, 2010; Timmermans and others, 2011; Jackson and others, 2012; Timmermans, 2015). The second location, north of the Canadian Archipelago (80 N, 110 W), is in a region with less solar heat input. This is in a region identified as the last Arctic sea-ice refuge (Pfirman and Tremblay, 2009). The annual cumulative solar heat input to open ocean, ice and their sum from 1985 to 2014 are plotted for both locations in Figure 3.

Annual heat inputs were greater at the Beaufort Sea site than the Canadian Archipelago site for the open ocean, ice and the combination in every year. While there was considerable interannual variability, there is an increasing trend of a few percent per year over the entire period of record for the Beaufort site. The trend for heat entering the open ocean (3.9% a^{-1}) was larger than the trend for heat entering through the ice (3.2% a^{-1}). The annual contribution of heat entering the open ocean to the total solar heat input to the ocean ranged from 57 to 94%, with an average of 79%.

At the Archipelago site, there were only modest variations until 2005, when the solar heat input through the ice and into

https://doi.org/10.1017/aog.2020.62 Published online by Cambridge University Press

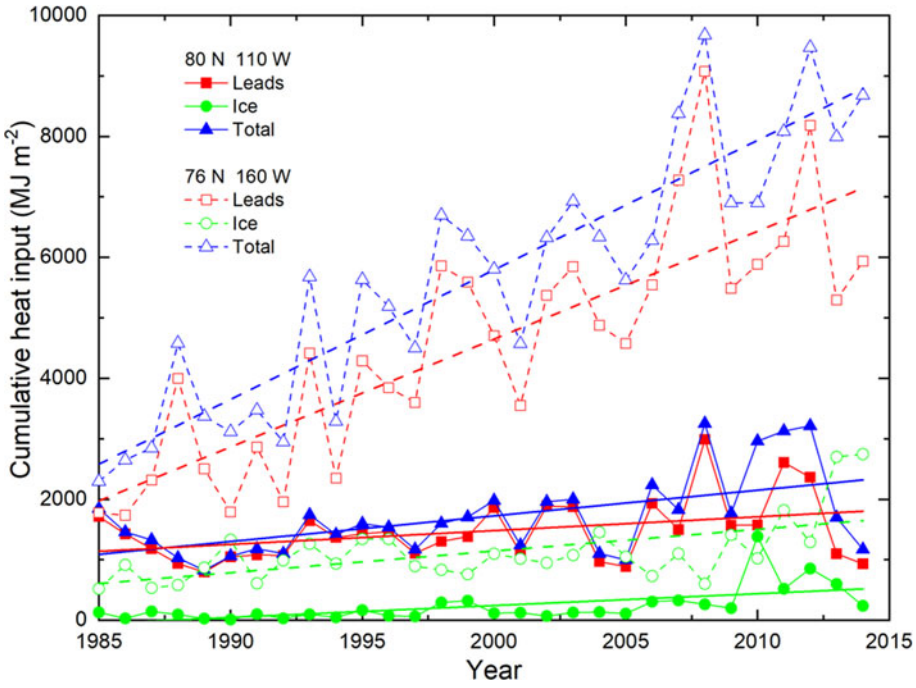

Fig. 3. Time series of annual solar heat input to the ocean for the Beaufort and Archipelago sites.

Table 1. Summary of linear trends and coefficient of determination (R^2) for annual solar heat input to the ocean into the open ocean, through ice and the combined total at locations in the Beaufort Sea and Canadian Archipelago

	Beaufort		Archipelago	
	Trend (% a^{-1})	R^2	Trend	R^2
Into open ocean	3.9	0.8	1.6	0.12
Through ice	3.2	0.33	3.4	0.34
Total	3.8	0.67	2.5	0.28

open ocean started to increase. In contrast to the Beaufort site, the trend in solar heat through the ice (3.4% a^{-1}) was much larger than the trend for heating directly into open ocean (1.6% a^{-1}). The trends and regression coefficients for the open ocean, ice and the sum for the two sites are summarized in Table 1. Open ocean dominated the annual solar heat to the ocean, with a contribution ranging from 53 to 99% and averaging 88%.

There was some spatial connection in the variations in annual solar heat input to the ocean at the two sites, with a correlation coefficient of 0.65. The Beaufort site averaged 3.5 times as much annual solar input to the ocean compared to the Archipelago site, ranging from 1.2 times in the first year of the record to 7.4 times in the last year.

Two of the six parameters in Eqn (1) are fixed: the open ocean albedo (0.07) and the extinction coefficient of ice (1.0 m^{-1}). That leaves four parameters as possible drivers of spatial and temporal changes: incident solar radiation, ice concentration, ice albedo and ice thickness. Solar radiation and ice concentration affect the contribution from both the open ocean and the ice. Ice albedo and ice thickness only impact the ice contribution. Temporal changes at the two sites for these four parameters are explored in Figure 4a–h. Each plot shows a year-by-year, day-by-day time series for one of the parameters at one of the sites. The horizontal axis is from 1 May to 30 September and the vertical axis is from 1985 (top) to 2014 (bottom).

The daily incoming solar heat displays a seasonal pattern at both sites, with peak values in June and early July, and a decrease through September. There is also day-to-day variability as shown in the speckles scattered about in the plots, due to changing cloud conditions. There is some modest year-to-year variability in these data, but no long term trend. Thus the daily incoming solar heat does not appear to be contributing to the observed 30-year trends in ocean heating.

The ice concentration plots show a general seasonal change at both sites, with decreasing concentration as summer progresses. There have been extreme changes over the years at the Beaufort site. In 1985, minimum ice concentration in summer was still above 0.8. Moving forward in time to the 1990s, there were periods in late summer when ice concentrations dropped to 0.5. This merely foreshadowed the extreme decreases of the 2000s, when it was typical for the Beaufort site to be ice-free from August through September. This decrease in summer ice concentration is the primary cause for the temporal increase in solar heat input to the ocean from the open ocean.

Change at the Archipelago site was much less pronounced. There were year-to-year fluctuations in July to September ice concentration, but no ice-free periods. A close examination shows longer periods in the summer in recent years with concentrations from 0.8 to 0.9 and occasional instances with concentrations as low as 0.6. As a result, there were only modest increases in the solar heat input through open ocean at the Archipelago site.

The solar heat input through the ice into the ocean is determined by the amount of incoming solar radiation, the ice concentration and additionally the albedo of the ice cover and its thickness. For both sites, there is a seasonal cycle of large albedo (0.85) in the spring, decreasing throughout the summer and then increasing again at the end of summer into the fall (Fig. 4e, f). The black area in Figure 4e represents the ice-free period that occurred at the Beaufort site. The beginning and the end of the smaller albedo period are controlled by the timing of the onsets of melt and of freeze-up. The wiggles in the albedo plots are due to variations in these onset dates. In addition to the interannual variability, the Beaufort site showed a trend towards a longer melt season and period of reduced albedo. In some recent years, the albedo did not return to spring values of 0.85 even by the end of September.

The Archipelago site shows the same interannual variability as the Beaufort site. However, the Archipelago site had shorter melt seasons and never had albedos as small as those at the Beaufort site. There has been some lengthening of the melt season at this site, with melt starting earlier in recent years.

https://doi.org/10.1017/aog.2020.62 Published online by Cambridge University Press

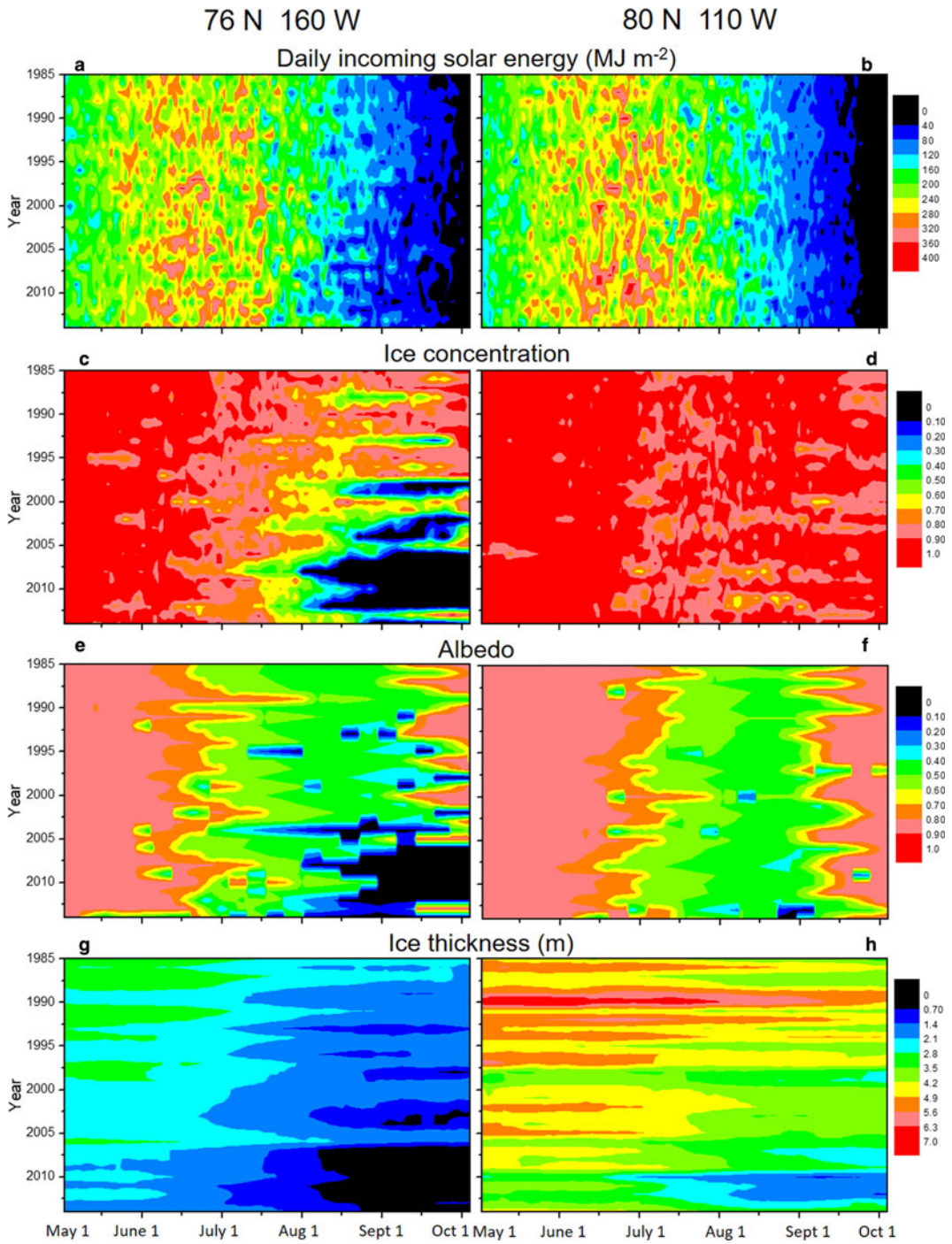

Fig. 4. Values of daily incoming solar heat (a, b); ice concentration (c, d); ice cover albedo (e, f); and ice thickness (g, h) for the Beaufort and Archipelago sites. Each panel presents daily results from 1 May to 30 September along the horizontal axis and from 1985 to 2014 along the vertical axis.

The striking differences in ice thickness (Fig. 4g, h) show differences in the seasonal cycle, interannual variability and trends from 1985 to 2014. In any given year, the seasonal cycle results in thinning ice during the summer melt season, with losses as large as 2 m. At the Beaufort site average May ice thickness was ~3.5 m in the 1980s and ~1.8 m at the end of summer melt. By the 2010s, the ice thickness was only 2.0–2.5 m in May and the ice had completely melted by the end of August.

The ice at the Archipelago site was thicker than the Beaufort site for every day of every year. In the 1980s and 1990s, May ice was 4–7 m thick. There is negligible solar heat transmitted through ice this thick. Even at the end of summer melt, the ice was usually thicker than 3.5 m. By the 2010s, the peak May thickness was only ~3 m and the summer minimum ranged from ~1.3 to 3 m. This thinning ice results in a corresponding exponential increase in the sunlight transmitted through the ice into the ocean.

Discussion and conclusions

Analysis of pan-Arctic results shows increasing trends in solar heat input to the upper ocean, with contributions from both inputs to the open ocean and transmission through the ice. To explore the drivers of these changes, we first focus on the results from the two sites presented in the results section.

The data from these two locations provide insight into the drivers of the trends in solar heat into the ocean. Changes in incoming solar energy can cause day-to-day and interannual

https://doi.org/10.1017/aog.2020.62 Published online by Cambridge University Press

fluctuations, but the incoming solar energy does not substantially contribute to the observed trends.

The solar heat input to the open ocean depends on the incoming solar energy and ice concentration. With no significant trend in incoming solar energy, Eqn (1) dictates that any trends in solar heat input into the open ocean are a direct consequence of trends in ice concentration. Indeed, this is clearly the case for both the Beaufort and Archipelago sites. The Beaufort site has seen a significant decline in ice concentration over the years, including ice-free months in summer. This has resulted in an increasing trend of 3.9% a^{-1} in solar heat input. In contrast, decreases in ice concentration were much smaller at the Archipelago site and the trend in solar heat input through open ocean was only 1.6% a^{-1}.

Examining the solar heat input through the ice is more complex, as it includes albedo and thickness of the ice cover as well as incoming solar radiation and ice concentration. At the Beaufort site, there were large decreasing trends in both albedo and thickness resulting in increased light transmission through the ice. However, the contribution from transmission through the ice was tempered by the decrease in ice concentration with time. The trends of decreasing solar heat transmitted through the ice are mainly around the periphery of the ice cover. These areas have seen significant reductions in the summer ice concentration. Less ice has resulted in a smaller contribution from light transmitted through the ice.

At the Archipelago location, the decrease in albedo was smaller than at the Beaufort location. There was a substantial decrease in ice thickness over the observation period, though peak values of transmittance were only a few percent. Summer ice concentrations were typically >0.8. Combining an increase in light transmittance with only a small decrease in concentration resulted in an increasing trend of ocean heat of 3.4% a^{-1} at the Archipelago locations, slightly larger than at the Beaufort locations.

The preceding discussion focused on two locations. The same basic principles and processes apply to interpret the entire dataset. There is a general increase in solar heat input to the ocean over most of the area where sea ice is present due to widespread and consistent decreases in ice concentrations. In the Central Arctic, north of the Canadian Archipelago, the thinning of the ice cover over the past few decades has resulted in substantial increases in the amount of sunlight transmitted through the ice. The total amount of heat transmitted through the ice depends on K, however, the trends are independent of this value.

There are several steps that can be taken to expand this analysis. The data record could be extended from 2014 to the present. Satellite-based observations of ice thickness from CryoSat-2, ICESat and ICESat-2 could be incorporated. Visible imagery could be used as reference points for the albedo evolution algorithm. More robust treatment of light transmission through the ice could be made, in particular, including the effects of spring snow, early summer melting snow and melt ponds. Such treatment would result in a temporally varying seasonal extinction coefficient, similar to the albedo evolution that was employed in this study. An extinction evolution based on the timing of snowmelt and pond development would be particularly useful for leveraging the results of Katlein and others (2019), This last point highlights the need to develop the explicit treatment of melt ponds. Melt ponds are implicitly included in the evolution of albedo. However, they are not considered in evaluating transmission through the ice. Because of the enhanced light transmission through ponds, including them would significantly increase the amount of light transmitted through the ice (Light and others, 2008, 2015; Arntsen, 2018).

Acknowledgements. Thanks to K.F. Jones for data contributions. This work was funded by the National Science Foundation and the Office of Naval Research.

References

Arndt S and Nicolaus M (2014) Seasonal cycle and long-term trend of solar energy fluxes through Arctic sea ice. *The Cryosphere* **8**, 2219–2233. doi: 10.5194/tc-8-2219-2014.

Arntsen AE (2018) *Impacts of Changing Sea Ice in the Beaufort and Chukchi Seas* (Ph.D. thesis), Dartmouth College, Hanover, NH, 127 pp.

Comiso JC (2012) Large decadal decline of the Arctic multiyear ice cover. *Journal of Climate* **25**(4), 1176–1193. doi: 10.1175/JCLI-D-11-00113.1.

Haynes J (2010) *Understanding the Importance of Oceanic Forcing on Sea Ice Variability* (Master's thesis), U.S. Naval Postgraduate School, 152 pp.

Hutchings JK and Rigor IG (2012) Role of ice dynamics in anomalous ice conditions in the Beaufort Sea during 2006 and 2007. *Journal of Geophysical Research* **117**(5), 1–14. doi: 10.1029/2011JC007182.

Jackson JM, Williams W and Carmack E (2012) Winter sea-ice melt in the Canada basin, Arctic ocean. *Geophysical Research Letters* **39**, 3. doi: 10.1029/2011GL050219.

Katlein C, Arndt S, Belter H, Castellani G and Nicolaus M (2019) Seasonal evolution of light transmission distributions through Arctic sea ice. *Journal of Geophysical Research* **124**, 5418–5435. https://doi.org/10.1029/2018JC014833.

Kay JE and Gettelman A (2009) Cloud influence on and response to seasonal Arctic sea ice loss. *Journal of Geophysical Research* **114**(18), 1–18. doi: 10.1029/2009JD011773.

King J and 6 others (2017) Sea-ice thickness from field measurements in the northwestern Barents sea. *Journal of Geophysical Research* **1**, 1497–1512.

Kwok R (2018) Arctic Sea ice thickness, volume, and multiyear ice coverage: losses and coupled variability (1958–2018). *Environmental Research Letters* **13**, 105005. doi: 10.1088/1748-9326/aae3ec.

Kwok R and 5 others (2019) Surface height and sea ice freeboard of the Arctic ocean from ICESat-2: characteristics and early results. *Journal of Geophysical Research* **124**, 6942–6959. doi: 10.1029/2019JC015486.

Light B, Grenfell TC and Perovich DK (2008) Transmission and absorption of solar radiation by Arctic sea ice during the melt season. *Journal of Geophysical Research* **113**, C03023. doi: 10.1029/2006JC003977.

Light B, Perovich DK, Webster MA, Polashenski CM and Dadic R (2015) Optical properties of melting first-year Arctic sea ice. *Journal of Geophysical Research-Oceans* **120**, 7657–7675. doi: 10.1002/2015JC011163.

Markus T, Stroeve JC and Miller J (2009) Recent changes in Arctic sea ice melt onset, freezeup, and melt season length. *Journal of Geophysical Research* **114,** C12024, 1–14. doi: 10.1029/2009JC005436.

Maslanik J, Stroeve J, Fowler C and Emery W (2011) Distribution and trends in Arctic sea ice age through spring 2011. *Geophysical Research Letters* **38** (13), L13502, 1–6. doi: 10.1029/2011GL047735.

Meier WN and others (2014) Arctic Sea ice in transformation: a review of recent observed changes and impacts on biology and human activity. *Reviews of Geophysics* **52**, 185–217. doi: 10.1002/2013RG000431.

Nicolaus M, Katlein C, Maslanik J and Hendricks S (2012) Changes in Arctic sea ice result in increasing light transmittance and absorption. *Geophysical Research Letters* **39**, L24501, 1–6. doi: 10.1029/2012GL053738.

Overland JE and Wang M (2005) The third Arctic climate pattern: 1930s and early 2000s. *Journal of Geophysical Research* **32**, L23808, 1-4. doi: 10.1029/2005GL024254.

Pegau WS and Paulson CA (2001) The albedo of Arctic leads in summer. *Annals of Glaciology* **33**, 221–224.

Perovich DK (2005) On the aggregate-scale partitioning of solar radiation in Arctic Sea Ice during the SHEBA field experiment. *Journal of Geophysical Research* **110**, C03002, 1–12. doi: 10.1029/2004JC002512.

Perovich, DK and 8 others (2011) Arctic Sea ice melt in 2008 and the role of solar heating, *Annals of Glaciology* **52**, 355–359.

Perovich DK, Grenfell TC, Light B and Hobbs PV (2002) The seasonal evolution of Arctic sea ice albedo. *Journal of Geophysical Research* **52**, 20-1–20-13. doi: 10.1029/2000JC000438.

Perovich DK and Polashenski C (2012) Albedo evolution of seasonal Arctic sea ice. *Geophysical Research Letters* **39**, L08501. doi: 10.1029/2012GL051432.

Perovich D, Richter-Menge JA, Jones KF and Light B (2008) Sunlight, water, and ice: extreme Arctic sea ice melt during the summer of 2007. *Geophysical Research Letters* **35**(11), 2–5. doi: 10.1029/2008GL034007.

Pfirman S and Tremblay B (2009) Arctic Refuge holds key to future of polar species. *New Scientist*, **204**, 26–27. doi: 10.1016/S0262-4079(09)62870-0.

Richter-Menge JA and others (2018) The Arctic (in "State of the Climate in 2017"). *Bulletin of the American Meteorological Society* **99**, 147–149. doi: 10.1175/2018BAMS.

Schweiger A and Zhang J (2015) Accuracy of short-term sea ice drift forecasts using a coupled ice-ocean model. *Journal of Geophysical Research: Oceans* **120**, 7827–7841. https://doi.org/10.1002/2015JC011237.

Serreze MC, Barrett AP, Stroeve JC, Kindig DN and Holland MM (2009). The emergence of surface-based Arctic amplification. *The Cryosphere* **3**, 11–19.

Stroeve JC and 6 others (2012) Trends in Arctic sea ice extent from CMIP5, CMIP3 and observations. *Geophysical Research Letters* **39**(16), 1–7. doi: 10.1029/2012GL052676.

Timmermans M-L and 6 others (2011) Surface freshening in the Arctic ocean's Eurasian basin: an apparent consequence of recent change in the wind-driven circulation. *Journal of Geophysical Research* **116**, C00D03, doi: 10.1029/2011JC006975.

Timmermans M-L (2015) The impact of stored solar heat on Arctic sea ice growth. *Geophysical Research Letters* **42**, 6399–6406. doi: 10.1002/2015GL064541.

Toole JM and 5 others (2010) Influences of the ocean surface mixed layer and thermohaline stratification on Arctic sea ice in the central Canada basin. *Journal of Geophysical Research* **115**, C10018. doi: 10.1029/2009JC005660.

Tschudi M, Meier WN, Stewart JS, Fowler C and Maslanik J (2019) EASE-Grid Sea Ice Age, Version 4. [Indicate subset used]. Boulder, Colorado USA. NASA National Snow and Ice Data Center Distributed Active Archive Center. doi: 10.5067/UTAV7490FEPB.

Tschudi MA, Stroeve JC and Stewart JS (2016) Relating the age of Arctic sea ice to its thickness, as measured during NASA's ICESat and Ice Bridge campaigns. *Remote Sensing* **8**(6), 1–13. doi: 10.3390/rs8060457.

Uttal T and others (2002) Surface heat budget of the Arctic ocean. *Bulletin of the American Meteorological Society* **83**, 255–275.

Zhang J and Rothrock DA (2003) Modeling global sea ice with a thickness and enthalpy distribution model in generalized curvilinear coordinates. *Monthly Weather Review* **131**(5), 845–861. doi: 10.1175/1520-0493.

Zhang J and 10 others (2016) The Beaufort gyre intensification and stabilization: a model-observation synthesis. *Journal of Geophysical Research: Oceans* **121**, 7933–7952. https://doi.org/10.1002/2016JC01219.

https://doi.org/10.1017/aog.2020.62 Published online by Cambridge University Press